Journal of Applied Physics

Hole capture-coefficient of intrinsic nonradiative recombination centers that commonly exist in bulk, epitaxial, and proton-irradiated ZnO

Cite as: J. Appl. Phys. **127**, 215704 (2020); https://doi.org/10.1063/5.0011309
Submitted: 22 April 2020 • Accepted: 23 May 2020 • Published Online: 04 June 2020

Shigefusa F. Chichibu, Akira Uedono, Kazunobu Kojima, et al.

Journal of Applied Physics ARTICLE scitation.org/journal/jap

Hole capture-coefficient of intrinsic nonradiative recombination centers that commonly exist in bulk, epitaxial, and proton-irradiated ZnO

Cite as: J. Appl. Phys. **127**, 215704 (2020); doi: 10.1063/5.0011309
Submitted: 22 April 2020 · Accepted: 23 May 2020 ·
Published Online: 4 June 2020

Shigefusa F. Chichibu,[1,a)] Akira Uedono,[2] Kazunobu Kojima,[1] Kazuto Koike,[3] Mitsuaki Yano,[3] Shun-ichi Gonda,[4] and Shoji Ishibashi[5]

AFFILIATIONS

[1]Institute of Multidisciplinary Research for Advanced Materials, Tohoku University, Sendai, Miyagi 980-8577, Japan
[2]Division of Applied Physics, Faculty of Pure and Applied Sciences, University of Tsukuba, Tsukuba, Ibaraki 305-8573, Japan
[3]Nanomaterials and Microdevices Research Center, Osaka Institute of Technology, Asahi-ku, Osaka 535-8585, Japan
[4]The Institute of Scientific and Industrial Research, Osaka University, Ibaraki, Osaka 567-0047, Japan
[5]Research Center for Computational Design of Advanced Functional Materials, National Institute of Advanced Industrial Science and Technology, Tsukuba, Ibaraki 305-8568, Japan

[a)]**Author to whom correspondence should be addressed:** chichibulab@yahoo.co.jp

ABSTRACT

Wurtzite ZnO and related $Mg_xZn_{1-x}O$ alloys are attractive semiconductors for the use in radiation-resistant and/or visible-light-transparent transistors and ultraviolet light-emitters. As free-carrier lifetime controls the device performances, the accurate understanding of the carrier capture-coefficients of dominant nonradiative recombination channels is essential. In this paper, the hole capture-coefficient (C_p) at room temperature of major intrinsic nonradiative recombination centers (NRCs) that commonly exist in various low dislocation density n-type epitaxial films and nearly dislocation-free bulk single crystals of ZnO with and without irradiation by an 8 MeV proton beam is determined. A two-component density functional theory calculation with positron annihilation measurement reveals that major vacancy-type defects are divacancies comprised of a Zn-vacancy and an O-vacancy ($V_{Zn}V_O$). Because the weak-excitation nonradiative photoluminescence lifetime (τ_{NR}) decreases with increasing $V_{Zn}V_O$ concentration ($[V_{Zn}V_O]$), $V_{Zn}V_O$ are assigned as major NRCs in n-type ZnO. From the relationship between τ_{NR} and $[V_{Zn}V_O]$, the values of C_p and hole capture-cross section of $V_{Zn}V_O$ are obtained to be $3 \times 10^{-7}\,cm^3s^{-1}$ and $2 \times 10^{-14}\,cm^2$, respectively, according to the Shockley–Read–Hall approach. These values are an order of magnitude larger than those of 3*d* transition metals such as Ni or Mn but are comparable to those of major intrinsic NRCs in n-type GaN, i.e., divacancies comprised of a Ga-vacancy and a N-vacancy ($V_{Ga}V_N$), being $6 \times 10^{-7}\,cm^3s^{-1}$ and $7 \times 10^{-14}\,cm^2$, respectively [S. F. Chichibu, A. Uedono, K. Kojima, H. Ikeda, K. Fujito, S. Takashima, M. Edo, K. Ueno, and S. Ishibashi, J. Appl. Phys. **123**, 161413 (2018)].

I. INTRODUCTION

Wurtzite (WZ) ZnO and $Mg_xZn_{1-x}O$ alloys are excellent candidates for the potential use in visible and ultraviolet (UV) excitonic light-emitters[1,2] because of their large bandgap energy (E_g) and large exciton binding energy; e.g., 3.36 eV at 300 K (Ref. 3) and 59 meV,[4] respectively. In addition, $Mg_xZn_{1-x}O$/ZnO heterostructures are proper candidates for realizing radiation-resistant and/or visible-light-transparent thin-film-transistors[5,6] and heterostructure field-effect-transistors[7,8] since quantum Hall effects have been demonstrated at the $Mg_xZn_{1-x}O$/ZnO heterointerface.[9]

For designing such advanced devices, in-depth probing and control of a carrier lifetime, especially minority carrier lifetime ($\tau_{minority}$), at various excitation conditions are essential because $\tau_{minority}$ is the recombination lifetime and determines the minority-carrier diffusion length ($L_{minority}$) and eventually limits the performances of optical and electronic devices. For example, the internal

quantum efficiency (η_{int}) of a near-band-edge (NBE) emission of light-emitting diode (LED) materials is determined by the balance between the radiative and nonradiative recombination rates (R_R and R_{NR}, respectively),

$$\eta_{int} = \frac{R_R}{(R_R + R_{NR})} = \frac{1}{1 + \frac{\tau_R}{\tau_{NR}}}, \quad (1)$$

where τ_R and τ_{NR} are the radiative and nonradiative recombination lifetimes that are inverses of R_R and R_{NR}, respectively, at a given excitation density. Accordingly, long τ_{NR} is preferred for optical devices such as LEDs, laser diodes, and solar cells. Long τ_{NR} is also required for high break-down voltage power devices. In the case of a direct bandgap semiconductor like ZnO, $\tau_{minority}$ can be measured by using time-resolved photoluminescence (TRPL) measurement because the photoluminescence (PL) lifetime (τ_{PL}) of an NBE emission is equal to $\tau_{minority}$ under weak-excitation conditions. Here, τ_{PL} is expressed as

$$\tau_{PL}^{-1} = \tau_R^{-1} + \tau_{NR}^{-1}. \quad (2)$$

Because R_R reflects the radiative performance, τ_R of a semiconductor without inhomogeneous broadening is unique to a material when there is no quantum confinement. On the other hand, τ_{NR} is determined by several factors: there are substantial nonradiative recombination channels, namely, voids, domain boundaries, stacking faults (SFs), dislocations, impurities, and point defects with decreasing structural size. Among these, the importance of midgap nonradiative recombination centers (NRCs), most probably originating from point defects,[10,11] has been recognized[12–14] from the initial stage of a ZnO LED research,[1,2] because quite low threading-dislocation (TD) density, large-size, and highly pure ZnO substrates could be grown at low cost by hydrothermal (HT) technique.[15] In the case of minority-carrier recombination at NRCs, τ_{NR} is given according to the Shockley–Read–Hall (SRH) theory by

$$\tau_{NR} = R_{NR}^{-1} = (C_{minority} \cdot N_{NRC})^{-1}, \quad (3)$$

where $C_{minority}$ and N_{NRC} are the capture-coefficient and concentration of major NRCs, respectively. In n-type ZnO (n-ZnO), $C_{minority}$ corresponds to a hole capture-coefficient (C_p) and is a product of a hole capture-cross section (σ_p) and thermal velocity of a hole ($v_p = \sqrt{3k_BT/m_p}$), where k_B is the Boltzmann constant, T is the temperature, and m_p is the hole effective mass: $C_p = \sigma_p \cdot v_p$. Accordingly, the accurate understanding of the origin and C_p of major NRCs is essential for improving optoelectronic device performances.

With respect to intrinsic NRCs in ZnO, the authors have studied[11–14] various quality bulk and epitaxial ZnO by using complementary TRPL[12–14] and positron (e^+) annihilation spectroscopy (PAS) measurements[11–14] and have pointed out that certain vacancy-complexes containing a Zn-vacancy (V_{Zn}),[11] namely, $V_{Zn}X$,[12–14] where the defect species of X was unrevealed in 2005, were the origin of major intrinsic NRCs in ZnO, because τ_{NR} at room temperature decreased with increasing the concentration[11] of V_{Zn}. Very recently, high-purity HT-ZnO crystals[15] irradiated with an 8-MeV proton beam have also been studied[16] by using this complementary approach to find that major defect species introduced by proton irradiation was divacancies comprised of a V_{Zn} and an O-vacancy (V_O), namely, $V_{Zn}V_O$. However, consensus has not yet been built on the species, concentration, and capture-coefficient of dominant intrinsic NRCs created during the bulk and epitaxial growths and particle irradiations such as protons or ions.

In this paper, the results of complementary PAS and weak-excitation TRPL measurements on nearly TD-free as-grown bulk single crystals[15–18] and epitaxial films[12–14] of ZnO and HT-ZnO crystals irradiated by an 8-MeV proton beam[16] are compared with the result of a two-component density functional theory (TC-DFT) calculation to identify the origin and quantify C_p of major intrinsic NRCs in ZnO. The results of PAS measurement and TC-DFT calculation indicate that major vacancy-type defects that commonly exist in our n-type ZnO samples are not single V_{Zn} but $V_{Zn}V_O$. Because τ_{NR} of NBE emission at 300 K monotonically decreases with increasing concentration of $V_{Zn}V_O$ ($[V_{Zn}V_O]$), $V_{Zn}V_O$ are assigned as major NRCs in n-ZnO. From the relationship between τ_{NR} and $[V_{Zn}V_O]$, the values of C_p and σ_p of $V_{Zn}V_O$ are estimated to be 3×10^{-7} cm^{3}s^{-1} and 2×10^{-14} cm^2, respectively. The results are compared with those of 3*d* transition metals such as Ni or Mn in ZnO (Ref. 19) and major intrinsic NRCs in n-type GaN (n-GaN), i.e., divacancies comprised of a Ga-vacancy (V_{Ga}) and a N-vacancy (V_N), $V_{Ga}V_N$.[20]

II. EXPERIMENTS AND ANALYSES

The measured samples consisted of three categories. (i) Nearly TD-free bulk ZnO single crystals grown by HT[15] and chemical vapor transport (CVT)[17,18] methods. The HT-ZnO wafers[15] were grown at Tokyo Denpa Co. Ltd., and CVT-ZnO wafer[17,18] was grown at Eagle-Picher Corp. Representative structural, PL, and TRPL data have been given in Refs. 1 and 12–18. (ii) Approximately 1-μm-thick, very low TD density undoped or N-doped $(000\bar{1})$ O-polarity and (0001) Zn-polarity ZnO epitaxial films grown by combinatorial laser molecular-beam epitaxy[21] on a nearly lattice-matched (0001) $ScAlMgO_4$ (SCAM)[22] and a Zn-polarity HT-ZnO substrate,[15] respectively, between 570 and 800 °C. We note that SCAM has an in-plane lattice mismatch of 0.09% to ZnO. Approximately 1-μm-thick $(000\bar{1})$ O-polarity ZnO heteroepitaxial film[13,14] grown on a sapphire (Al_2O_3) substrate was also examined. Details of the epilayer growths are given in Refs. 21 and 22, and most of steady-state PL and TRPL data can be found in Refs. 12–14. (iii) Nearly TD-free, 330-μm-thick HT-ZnO wafers[15] that were irradiated with an 8-MeV proton (H^+) beam.[16] The proton dose was 4.2×10^{16} p · cm^{-2}. The wafers were purchased in 2012 after annealing at 1400 °C for removing Li impurities incorporated from the mineralizer and subsequent mirror-polishing. The electron concentration and mobility before irradiation were about 6×10^{14}–1×10^{15} cm^{-3} and 130 cm^2 V^{-1} s^{-1} at 300 K, respectively, meaning that the Fermi level is still located at a higher electron-energy position close to the conduction band. The proton beam irradiation was carried out at The Wakasawan Energy Research Center[23] for both (0001) Zn-polarity and $(000\bar{1})$ O-polarity c-planes.[15] Because distinct difference in defect or optical properties between Zn- and O-polarity ZnO was not found,[16] they are treated

as the same category in this paper. Details of the proton irradiation and fundamental PAS, PL, and TRPL data are given in Ref. 16. We note that the proton beam is expected to pass through the ZnO wafers since the ion track trajectory calculated for semi-infinite long ZnO by the SRIM code[24] reaches around 420 μm. The sample was annealed at 200 °C for 10 min in an O_2 atmosphere before PL and TRPL measurements.

For identifying the species and quantifying the concentration of major vacancy-type defects, a TC-DFT calculation was carried out to analyze the results of PAS measurement.[11–14,16] PAS[11,25–31] is an established, nondestructive, and exclusive tool to detect negatively charged and neutral vacancy defects in a semiconductor. e^+ is an antimatter of an electron (e^-) and has a positive charge with a mass (m) identical to e^-. When e^+ is implanted into the condensed matter, it annihilates with a surrounding e^- and emits two 511 keV γ-rays according to $E_\gamma = mc^2$, where E_γ is the energy and c is the speed of the light. The annihilating γ-ray spectra are broadened in energy due to the momentum distribution of the annihilating e^+–e^- pair p_L, which is parallel to the direction of the γ-rays. The energy of the γ-rays is given by $E_\gamma = mc^2 \pm \Delta E_\gamma$. The Doppler shift ΔE_γ is given by the relation $\Delta E_\gamma = p_L c/2$. A freely diffusing e^+ likely localize in a vacancy-type defect because of Coulomb repulsion from ion cores. As the momentum distribution of e^- surrounding such defects is smaller than that in defect-free (DF) delocalized regions, the defects can be detected by measuring the Doppler broadening spectra of the γ-rays. The resulting change in the γ-ray spectra is characterized by the line-shape parameter S and the wing parameter W, where the former mainly reflects the fraction of annihilating e^+–e^- pairs of small momentum distribution (mostly valence electrons) and the latter represents the fraction of the pairs of large momentum distribution (mostly core electrons). Since V_{Zn} and their complexes form acceptor-type defects in ZnO, they are the most probable candidates of e^+ trapping centers.[11,28] Accordingly, (S,W) coordinates can be used as a measure of species and concentration of V_{Zn} and V_{Zn}-complexes. For measuring the γ-ray spectra as a function of incident e^+ energy E, a monoenergetic e^+-beam line with the coincidence detection system[11,16,20,27] was used. A spectrum with 5×10^6 counts was measured using a Ge detector at each E. The S parameter was defined as the number of annihilation events for the energy range of 511 keV $\pm$ ΔE_γ, where $\Delta E_\gamma = 0.76$ keV, around the center of the peak, over the total counts. The W parameter was defined for the annihilation events in the tail of the same spectrum (3.4 keV $\leq |\Delta E_\gamma| \leq$ 6.8 keV) over the total counts. In this study, S and W values measured for $E > 15$ keV were used for bulk values.

In order to determine the species of defects, Doppler broadening spectra of the γ-rays were theoretically calculated using the QMAS (Quantum MAterials Simulator) code,[29–31] which uses valence–electron wavefunctions determined by the projector augmented-wave (PAW) method.[32,33] To describe the electronic exchange and correlation energies of electrons, the generalized gradient approximation[34] was used. The calculations were carried out on orthorhombic supercells equivalent to $4 \times 4 \times 2$ WZ cells containing 128 atoms when there exist no vacancies. The supercell dimensions were $2\sqrt{3}a_0 \times 4a_0 \times 2c_0$, where $a_0 = 0.3249$ nm and $c_0 = 0.5205$ nm are the lattice parameters. For the supercell containing a defect, atomic positions in the fixed cell (with the experimental lattice parameters) were computationally optimized. The formalism of the local density approximation[35,36] was used to describe the electron–positron correlation. Because localized e^+ at vacancy-type defects likely affect the defect configuration and hence the corresponding e^+ annihilation,[31,37] the effects caused by the trapped e^+ were taken into account by using the TC-DFT scheme.[35,36] The calculated atomic configurations of Zn and O atoms around a V_{Zn} monovacancy and a $V_{Zn}V_O$ divacancy with a trapped e^+ are schematically drawn in Figs. 1(a) and 1(b), respectively, by using VESTA.[38] In Fig. 1, density distributions of trapped e^+ are indicated by using the isosurfaces that correspond to 1/10 of the maximum densities. As shown, e^+ density is well localized at the vacancy sites. The Doppler broadening spectra resulted from the annihilation of e^+ in DF and several trapped states were calculated, and the directionally averaged (S,W) coordinates for e^+ annihilation at the DF region [(S_{DF}, W_{DF})], V_{Zn} [($S_{V_{Zn}}$, $W_{V_{Zn}}$)], $V_{Zn}V_O$ [($S_{V_{Zn}V_O}$, $W_{V_{Zn}V_O}$)], $V_{Zn}(V_O)_2$ trivacancies [($S_{V_{Zn}(V_O)_2}$, $W_{V_{Zn}(V_O)_2}$)], and $(V_{Zn}V_O)_2$ tetravacancies [($S_{(V_{Zn}V_O)_2}$, $W_{(V_{Zn}V_O)_2}$)] are shown by closed symbols in Fig. 2. Because the sizes of the open spaces of V_{Zn} and $V_{Zn}V_O$ are slightly different, the (S,W) coordinates for V_{Zn} and $V_{Zn}V_O$ are slightly but measurably different. We note that the present theoretical results of S and W are in good agreement with those reported in a preceding work[39] although stringent comparison is difficult because the definitions of S and W parameters are slightly different.

For TRPL measurement, the NBE PL was excited using approximately 200 fs pulses of a frequency-tripled (3ω) mode-locked Al_2O_3:Ti laser (267 nm) operating at 80 MHz. The excitation power density was 120 nJ cm^{-2} per pulse to ensure the

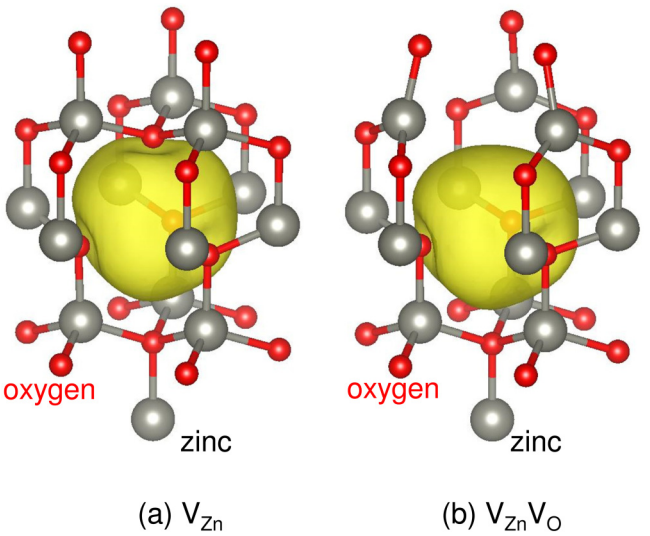

FIG. 1. Calculated atomic configurations of Zn and O atoms around (a) a V_{Zn} monovacancy and (b) a $V_{Zn}V_O$ divacancy with a trapped positron. In both panels, the density distributions of the trapped positron are indicated by using the isosurfaces that correspond to 1/10 of the maximum densities. These figures are drawn using VESTA.[38]

weak-excitation conditions. The spot diameter and estimated excited carrier concentration were 1 mm and a few times 10^{16} cm^{-3}, respectively, when τ_{PL} is 1 ns. The reason why TRPL was carried out under the weak-excitation regime was to underline the nonradiative recombination processes. The TRPL signal was collected using a standard streak camera, and the decay signal was fitted using a single- or bi-exponential line shape function: $I(t) = A_1 \exp(-t/\tau_1) + A_2 \exp(-t/\tau_2)$, where $I(t)$ is the intensity at time t and A_1 (A_2) and τ_1 (τ_2) are the pre-exponential constant and lifetime, respectively, of the fast (slow) decay component. The value of τ_1, which mostly limits the cw PL intensity at room temperature, is used as the representative τ_{PL}.

III. RESULTS AND DISCUSSION

The measured (S,W) for bulk ZnO single crystals,[11,16] ZnO epilayers,[11] and HT-ZnO after 4.2×10^{16} p · cm^{-2} proton irradiation with subsequent annealing at 200 °C for 10 min in O_2 are shown by a representative open circle, open triangles, and an open square, respectively, in Fig. 2. The experimental errors for the determination of both S and W were less than 0.1%, and therefore, the error bars are not given on the plots. Because (S,W) for the HT[16]- and CVT[11]-ZnO crystals were almost the same, their (S,W) are indicated by a single open circle as a representative plot. The (S,W) coordinates for ZnO epilayers[11] were properly calibrated for the present S–W gauge.

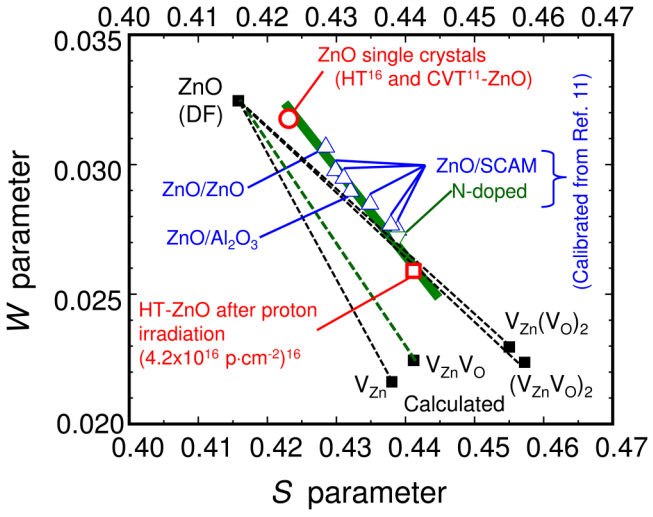

FIG. 2. S–W relationships for the bulk ZnO grown by HT[16] and CVT[11] methods (open circle as a representative), Zn- or O-polar ZnO epilayers (open triangles),[11] and HT-ZnO after 4.2×10^{16} p · cm^{-2} proton irradiation with subsequent annealing at 200 °C for 10 min in O_2 (open square).[16] The (S,W) values calculated using the QMAS code[29–31] for e^+ annihilation at the defect-free (DF) region, V_{Zn}, $V_{Zn}V_O$ divacancies, $V_{Zn}(V_O)_2$ trivacancies, and $(V_{Zn}V_O)_2$ tetravacancies are shown by closed symbols (this work). The experimental data appear to align close to the line connecting (S_{DF}, W_{DF}) and ($S_{V_{Zn}V_O}$, $W_{V_{Zn}V_O}$), implying that major vacancy-type defects in the present ZnO samples are $V_{Zn}V_O$. [Experimental data plots for HT- and CVT-ZnO are reproduced with permission from Koike *et al.*, J. Appl. Phys. **123**, 161562 (2018) and the plots for ZnO epilayers are imported and calibrated to fit the present gauge with permission from Uedono *et al.*, J. Appl. Phys. **93**, 2481 (2003). Copyright 2018 and 2003 AIP Publishing LLC.]

Because nearly TD-free HT- and CVT-ZnO showed the same, smallest S and largest W, and they generally exhibit long τ_{PL} for NBE emission of the order of 1 ns at room temperature,[12–14,40,41] $V_{Zn}X$ (Refs. 12–14) concentrations ([$V_{Zn}X$]) in them are less than or equal to the detection limit of PAS measurement (a few times 10^{15} cm^{-3}).[28] We note that the positron diffusion length (L_+) of approximately 50 nm for both HT-ZnO[16] and CVT-ZnO[11] also supports that the gross concentration of e^+ trapping and scattering centers (N_{defect}^{gross}), both decrease L_+, is likely lower than 10^{16} cm^{-3}, because three-dimensional (3D) average distance between adjacent such defects is 100 nm for $N_{defect}^{gross} = 10^{15}$ cm^{-3} and 46 nm for $N_{defect}^{gross} = 10^{16}$ cm^{-3}. Accordingly, the (S,W) coordinate obtained from these ZnO single crystals expresses the "experimental" (S_{DF}, W_{DF}). However, the measured (S,W) coordinate (open circle) lies to the lower right of the calculated (S_{DF}, W_{DF}) (closed square) in Fig. 2. This difference could be due to several reasons such as the limitations of first-principles calculations applied to Doppler broadening spectra, temperature dependent differences between the modeling and experimental conditions, the experimental background, and/or the energy resolutions of our Ge detectors.

When the samples contain mono-defects of vacancy-type, e^+ annihilate from the DF state or from the trapped (defect) state. In this case, (S,W) becomes a weighted average of (S_{DF}, W_{DF}) and (S_{defect}, W_{defect}), where S_{defect} and W_{defect} are characteristic S and W, respectively, of the defect. Accordingly, experimental (S,W) should lie on a line connecting (S_{DF}, W_{DF}) and (S_{defect}, W_{defect}). It should be noted that the slope of the line is more important to determine the defect species, as experimental data plots commonly suffer from above observed lower-right shifts. Taking the slope of the approximated line for the measured (S,W) of all samples (thick solid line in Fig. 2) into account, both V_{Zn} and $V_{Zn}V_O$ can be probable candidates for the major vacancy-type defects. However, since the experimental data appear to align closer on the line connecting (S_{DF}, W_{DF}) and ($S_{V_{Zn}V_O}$, $W_{V_{Zn}V_O}$) rather than that connecting (S_{DF}, W_{DF}) and ($S_{V_{Zn}}$, $W_{V_{Zn}}$), $V_{Zn}V_O$ are assigned as major intrinsic vacancy-type defects common to all ZnO. This result is interesting, as variety of samples grown by different methods might have different particular defects. Also, one would argue that the formation energies (E_{Form}) of V_{Zn} and V_O in n-ZnO differ substantially, because V_{Zn} and V_O are acceptor-type and donor-type vacancies, respectively, and E_{Form} would also vary depending on growth stoichiometry.[10] One of the plausible explanations for these questions is that a $V_{Zn}V_O$ divacancy is formed all together, having its unique E_{Form} and particular charge-transfer energy levels. After forming $V_{Zn}V_O$, $V_{Zn}V_O$ can agglomerate into larger vacancy clusters like $(V_{Zn}V_O)_2$, whose theoretical (S,W) coordinate lies to the lower right. We note that similar result has been found in the case of GaN: major intrinsic vacancy-type defects in n-type GaN of various orientations grown by various methods are $V_{Ga}V_N$.[20]

The dynamic range of PAS measurement for V_{Zn} in ZnO is approximately between a few times 10^{15} and a few times 10^{18} cm^{-3}, at which e^+ implanted in the sample is mostly delocalized in DF regions and mostly trapped by V_{Zn}, respectively.[28] Accordingly, the concentration of V_{Zn} ([V_{Zn}]) is lower than 10^{16} cm^{-3} for

(S_{DF}, W_{DF}) and higher than 10^{18} cm^{-3} for ($S_{V_{Zn}}$, $W_{V_{Zn}}$). In analogy, [$V_{Zn}V_O$] of the ZnO samples shown in Fig. 2 are in the range between a few times 10^{15} cm^{-3} and a few times 10^{17} cm^{-3}.

For finally identifying the origin and quantifying C_p of major intrinsic NRCs in ZnO, the values of τ_{PL} at 300 K for the ZnO samples are shown as a function of [$V_{Zn}V_O$] in Fig. 3 by using the same symbols used in Fig. 2. In Fig. 3, the right y axis shows corresponding η_{int} using $\tau_R = 20$ ns (Ref. 14) and x axis is a priori labeled as N_{NRC}. Three ideal τ_{PL} curves are drawn for the cases with σ_p ranging from 1×10^{-15} to 1×10^{-13} cm^2 using the relationship

$$\tau_{PL}^{-1} = \tau_R^{-1} + C_{minority} \cdot N_{NRC} = \tau_R^{-1} + \sigma_p \cdot \nu_p \cdot N_{NRC}, \quad (4)$$

where $\nu_p = 1.5 \times 10^7$ cm $\cdot$ s^{-1} and the hole effective mass $m_p = 0.60 m_0$ (m_0 is a free electron mass).[42] Equation (4) predicts that $\tau_{PL} - N_{NRC}$ shows a straight line under high N_{NRC} conditions, where τ_{NR} dominates τ_{PL}. Because the temporal resolution of our TRPL system was better than 1 ps and the dynamic range of the PAS measurement is approximately between a few times 10^{15} and a few times 10^{18} cm^{-3}, the data points in the shaded zone are practically reliable. As shown, the data points appear to align on the broken line that is drawn for $C_p = 3 \times 10^{-7}$ cm^{3}s^{-1} ($\sigma_p = 2 \times 10^{-14}$ cm^2). Because τ_{NR} decreases with increasing [$V_{Zn}V_O$], $V_{Zn}V_O$ are eventually assigned as major intrinsic NRCs in n-ZnO. An evidence to support this assignment is that isolated single V_{Zn} in ZnO has been assigned to form a radiative recombination center.[42] The value of C_p being 3×10^{-7} cm^{3}s^{-1} is about an order of magnitude larger than that of $Ni^{2+/3+}$ or $Mn^{2+/3+}$ (Ref. 19), of which τ_{PL} is shown by closed squares in Fig. 3. This result is not so amazing, as a $V_{Zn}V_O$ having the energy level at around the midgap would have larger trapping potential than that of substitutional transition metals (TMs). Also, the C_p and σ_p values of $V_{Zn}V_O$ in ZnO are close to those of $V_{Ga}V_N$, which are major NRCs in n-GaN,[20] being $C_p = 6 \times 10^{-7}$ cm^{3}s^{-1} and $\sigma_p = 7 \times 10^{-14}$ cm^2.

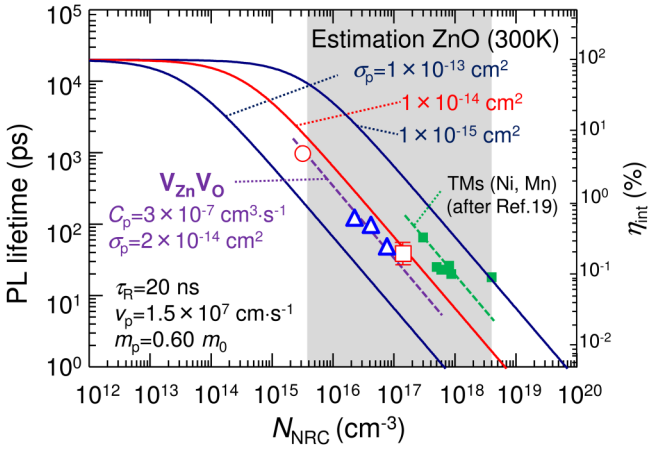

FIG. 3. PL lifetime τ_{PL} (left y axis) and corresponding η_{int} (right y axis) for NBE emission of n-ZnO samples at 300 K as a function of N_{NRC} ([$V_{Zn}V_O$] for the present ZnO samples). The value of η_{int} was derived using $\tau_R = 20$ ns (Ref. 14). Open circle shows the representative value for the bulk ZnO single crystals grown by HT and CVT methods, open triangles show the data for ZnO/SCAM epilayers, and an open square shows the data for HT-ZnO after 4.2×10^{16} p $\cdot$ cm^{-2} proton irradiation with subsequent annealing at 200 °C for 10 min in O_2. Three ideal τ_{PL} curves are drawn for the cases with σ_p ranging from 1×10^{-15} to 1×10^{-13} cm^2 using the relationship $\tau_{PL}^{-1} = \tau_R^{-1} + C_p \cdot N_{NRC} = \tau_R^{-1} + \sigma_p \cdot v_p \cdot N_{NRC}$, where $v_p = 1.5 \times 10^7$ cm $\cdot$ s^{-1} and $m_p = 0.60 m_0$.[42] As the temporal resolution of our TRPL system was better than 1 ps and the dynamic range of the present PAS measurement is approximately between a few times 10^{15} and a few times 10^{18} cm^{-3} in ZnO, the data points in the shaded zone are reliable. Such data points appear to align on the broken line drawn for $C_p = 3 \times 10^{-7}$ cm^{3}s^{-1} ($\sigma_p = 2 \times 10^{-14}$ cm^2). Because τ_{NR} decreases with increasing [$V_{Zn}V_O$], $V_{Zn}V_O$ are assigned as major intrinsic NRCs. The value of C_p being 3×10^{-7} cm^{3}s^{-1} is about an order of magnitude larger than that of $Ni^{2+/3+}$ or $Mn^{2+/3+}$ (Ref. 19), of which τ_{PL} is shown by closed squares. [The reference data for TMs such as $Ni^{2+/3+}$ or $Mn^{2+/3+}$ shown by closed squares are reproduced with permission from Chichibu *et al.*, Appl. Phys. Lett. **108**, 021904 (2016). Copyright 2016 AIP Publishing LLC.]

IV. CONCLUSION

In this paper, the results of complementary PAS and weak-excitation TRPL measurements on nearly TD-free bulk single crystals, epitaxial films, and 8-MeV proton irradiated ZnO samples were compared with the results of the TC-DFT calculation to eventually assign $V_{Zn}V_O$ divacancies as major vacancy-type defects in n-ZnO samples. As τ_{NR} of the NBE emission at 300 K monotonically decreased with increasing [$V_{Zn}V_O$], $V_{Zn}V_O$ are assigned as major NRCs in n-ZnO. From the relationship between τ_{NR} and [$V_{Zn}V_O$], the values of C_p and σ_p for $V_{Zn}V_O$ are estimated to be 3×10^{-7} cm^{3}s^{-1} and 2×10^{-14} cm^2, respectively, according to the SRH approach. These values are an order of magnitude larger than those of 3d TMs such as Ni or Mn but are comparable to those of major intrinsic NRCs in n-GaN, i.e., 6×10^{-7} cm^{3}s^{-1} and 7×10^{-14} cm^2, respectively, of $V_{Ga}V_N$ divacancies.[20]

ACKNOWLEDGMENTS

The authors thank Professor M. Kawasaki, Professor A. Ohtomo, and Professor A. Tsukazaki for providing the ZnO epilayers, Dr. R. Ishigami and Dr. K. Kume at The Wakasawan Energy Research Center for the professional help with the proton beam irradiation, and T. Ohtomo at Tohoku University for help with the experiments. This work was supported in part by the Cooperative Research Program of "Network Joint Research Center for Materials and Devices" and "Dynamic Alliance for Open Innovation Bridging Human, Environment and Materials" by MEXT, Japan.

DATA AVAILABILITY

The data that support the findings of this study are available within this article and openly available in publications in American Institute of Physics, Refs. 11, 16, and 19.

REFERENCES

[1]A. Tsukazaki, A. Ohtomo, T. Onuma, M. Ohtani, T. Makino, M. Sumiya, K. Ohtani, S. F. Chichibu, S. Fuke, Y. Segawa, H. Ohno, H. Koinuma, and M. Kawasaki, Nat. Mater. **4**, 42 (2005).
[2]K. Nakahara, S. Akasaka, H. Yuji, K. Tamura, T. Fujii, Y. Nishimoto, D. Takamizu, A. Sasaki, T. Tanabe, H. Takasu, H. Amaike, T. Onuma,

S. F. Chichibu, A. Tsukazaki, A. Ohtomo, and M. Kawasaki, Appl. Phys. Lett. **97**, 013501 (2010).
[3]D. Reynolds, D. Look, B. Jogai, and H. Morkoc, Solid State Commun. **101**, 643 (1997).
[4]D. G. Thomas, J. Phys. Chem. Solids **15**, 86 (1960).
[5]P. F. Carcia, R. S. McLean, M. H. Reilly, and G. Nunes, Jr., Appl. Phys. Lett. **82**, 1117 (2003).
[6]S. Masuda, K. Kitamura, Y. Okumura, S. Miyatake, H. Tabata, and T. Kawai, J. Appl. Phys. **93**, 1624 (2003).
[7]S. Sasa, T. Hayafuji, M. Kawasaki, K. Koike, M. Yano, and M. Inoue, Jpn. J. Appl. Phys. **47**, 2845 (2008).
[8]A. Tsukazaki, H. Yuji, S. Akasaka, K. Tamura, K. Nakahara, T. Tanabe, H. Takasu, A. Ohtomo, and M. Kawasaki, Appl. Phys. Express **1**, 055004 (2008).
[9]A. Tsukazaki, A. Ohtomo, T. Kita, Y. Ohno, H. Ohno, and M. Kawasaki, Science **315**, 1388 (2007).
[10]A. F. Kohan, G. Ceder, D. Morgan, and C. G. Van de Walle, Phys. Rev. B **61**, 15019 (2000).
[11]A. Uedono, T. Koida, A. Tsukazaki, M. Kawasaki, Z. Q. Chen, S. F. Chichibu, and H. Koinuma, J. Appl. Phys. **93**, 2481 (2003).
[12]T. Koida, S. F. Chichibu, A. Uedono, A. Tsukazaki, M. Kawasaki, T. Sota, Y. Segawa, and H. Koinuma, Appl. Phys. Lett. **82**, 532 (2003).
[13]S. F. Chichibu, A. Uedono, A. Tsukazaki, T. Onuma, M. Zamfirescu, A. Ohtomo, A. Kavokin, G. Cantwell, C. W. Litton, T. Sota, and M. Kawasaki, Semicond. Sci. Technol. **20**, S67 (2005).
[14]S. F. Chichibu, T. Onuma, M. Kubota, A. Uedono, T. Sota, A. Tsukazaki, A. Ohtomo, and M. Kawasaki, J. Appl. Phys. **99**, 093505 (2006).
[15]E. Ohshima, H. Ogino, I. Niikura, K. Maeda, M. Sato, M. Ito, and T. Fukuda, J. Cryst. Growth **260**, 166 (2004).
[16]K. Koike, W. Kuwagata, H. Mito, M. Yano, S. Gonda, A. Uedono, S. Ishibashi, K. Kojima, and S. F. Chichibu, J. Appl. Phys. **123**, 161562 (2018).
[17]D. C. Look, D. C. Reynolds, J. R. Sizelove, R. L. Jones, C. W. Litton, G. Cantwell, and W. C. Harsch, Solid State Commun. **105**, 399 (1998).
[18]S. F. Chichibu, T. Sota, G. Cantwell, D. B. Eason, and C. W. Litton, J. Appl. Phys. **93**, 756 (2003).
[19]S. F. Chichibu, K. Kojima, Y. Yamazaki, K. Furusawa, and A. Uedono, Appl. Phys. Lett. **108**, 021904 (2016).
[20]S. F. Chichibu, A. Uedono, K. Kojima, H. Ikeda, K. Fujito, S. Takashima, M. Edo, K. Ueno, and S. Ishibashi, J. Appl. Phys. **123**, 161413 (2018).
[21]T. Ohnishi, D. Komiyama, T. Koida, S. Ohashi, C. Stauter, H. Koinuma, A. Ohtomo, M. Lippmaa, N. Nakagawa, M. Kawasaki, T. Kikuchi, and K. Omote, Appl. Phys. Lett. **79**, 536 (2001).
[22]A. Ohtomo, K. Tamura, K. Saikusa, K. Takahashi, T. Makino, Y. Segawa, H. Koinuma, and M. Kawasaki, Appl. Phys. Lett. **75**, 2635 (1999).
[23]See http://www.werc.or.jp/ for The Wakasawan Energy Research Center.
[24]See http://www.srim.org/ for SRIM simulation.
[25]R. Krause-Rehberg and H. S. Leipner, *Positron Annihilation in Semiconductors: Defect Studies* (Springer-Verlag, Berlin, 1999), Vol. 127.
[26]P. G. Coleman, *Positron Beams and Their Application* (World Scientific, Singapore, 2000).
[27]A. Uedono, S. Ishibashi, T. Ohdaira, and R. Suzuki, J. Cryst. Growth **311**, 3075 (2009).
[28]F. Tuomisto and I. Makkonen, Rev. Mod. Phys. **85**, 1583 (2013).
[29]S. Ishibashi, Mater. Sci. Forum **445–446**, 401 (2004).
[30]S. Ishibashi, T. Tamura, S. Tanaka, M. Kohyama, and K. Terakura, Phys. Rev. B **76**, 153310 (2007).
[31]S. Ishibashi and A. Uedono, J. Phys. Conf. Ser. **505**, 012010 (2014).
[32]P. E. Blöchl, Phys. Rev. B **50**, 17953 (1994).
[33]G. Kresse and D. Joubert, Phys. Rev. B **59**, 1758 (1999).
[34]J. P. Perdew, K. Burke, and M. Ernzerhof, Phys. Rev. Lett. **77**, 3865 (1996).
[35]E. Boronski and R. M. Nieminen, Phys. Rev. B **34**, 3820 (1986).
[36]M. J. Puska, A. P. Seitsonen, and R. M. Nieminen, Phys. Rev. B **52**, 10947 (1995).
[37]S. Ishibashi, Acta Phys. Pol. A **132**, 1602 (2017).
[38]K. Momma and F. Izumi, J. Appl. Crystallogr. **44**, 1272 (2011).
[39]I. Makkoń en, E. Korhonen, V. Prozheeva, and F. Tuomisto, J. Phys. Condens. Matter **28**, 224002 (2016).
[40]A. Teke, U. Oezguer, S. Dogan, X. Gu, H. Morkoc, B. Nemeth, J. Nause, and H. O. Everitt, Phys. Rev. B **70**, 195207 (2004).
[41]U. Oezguer, Y. I. Alivov, C. Liu, A. Teke, M. A. Reshchikov, S. Dogan, V. Avrutin, S.-J. Cao, and H. Morkoc, J. Appl. Phys. **98**, 041301 (2005).
[42]C. Klingshirn, Phys. Status Solidi B **244**, 3027 (2007).